

Support information

Anti-swelling dual-network zwitterionic hydrogels with excellent mechanical properties for flexible supercapacitors and sensors

Mengmeng Xun^a, Xiaoyan Li^a, Kanjun Sun^b, Xuan Xie^a, Hui Peng^a, Guofu Ma^{a*}, Yuxi Xu^{*c}

^aKey Laboratory of Eco-functional Polymer Materials of the Ministry of Education, Key Laboratory of Polymer Materials of Gansu Province, College of Chemistry and Chemical Engineering, College of Engineering, Northwest Normal University, Lanzhou 730070, China

^bCollege of Chemistry and Chemical Engineering, Lanzhou City University, Lanzhou 730070, China

^cSchool of Engineering, Westlake University, Hangzhou 310024, China.

*Corresponding authors. magf@nwnu.edu.cn (G. Ma), xuyuxi@westlake.edu.cn (Y. Xu).

S1. Experimental section

S1.1 Materials

Polyvinyl alcohol (PVA, 1799), 2-(methacryloyloxy)ethyl]dimethyl-(3-sulfopropyl)ammonium hydroxide (SBMA), phytic acid (PA, 70%), lithium sulfate (Li_2SO_4), and potassium persulfate (KPS) were purchased from Tianjin Kaixin Chemical Industry Co. Activated carbon (AC, YP-80) with the specific surface area of $2100 \text{ m}^2 \text{ g}^{-1}$ was purchased from Kuraray Japan. Acetylene black (AB), Polyvinylidene fluoride (PVDF). All the reagents are of analytical grade and used without further purification.

S1.2 Preparation of the PVA/PSBMA-PA- Li_2SO_4 hydrogel

1.0 g of PVA was dissolved in water at $95 \text{ }^\circ\text{C}$ and cooled to $50 \text{ }^\circ\text{C}$, then 1.286 g of SBMA, appropriate amount of phytic acid (PA) and Li_2SO_4 were added to form a homogeneous and transparent solution. Subsequently, the 0.014 g (KPS) was added and mixed thoroughly, poured into the mould (10 cm x 1.5 cm x 2 cm) and then placed in the oven at $60 \text{ }^\circ\text{C}$ for 3 h. The hydrogel was subjected to three cycles of freezing ($-20 \text{ }^\circ\text{C}$, 3 h) and thawing.

For comparison, PVA/PSBMA-PA- Li_2SO_4 hydrogels with different PA content (15 wt%, 20 wt%, 25 wt%, 30 wt% relative to SBMA content) were prepared by the same method described above. In addition, the PVA/PSBMA-PA- Li_2SO_4 hydrogels with different content of Li_2SO_4 (0.3 g, 0.4 g, 0.5 g, 0.6 g) were also investigated.

S2. Fabrication of the supercapacitor

The 16 mg of activated carbon (AC, YP-80), 2 mg of acetylene black and 2 mg of polyvinylidene fluoride (PVDF) were dispersed in N-methyl-2-pyrrolidone (NMP) to form uniform slurry. Then, the slurry was coated on stainless steel meshes (2 cm x 1.5 cm) with the average mass of 8 mg, and dried at $60 \text{ }^\circ\text{C}$ for 8 h. Finally, a symmetric supercapacitor with sandwich structure (AC/hydrogel electrolyte/AC) was fabricated based on AC as electrode materials and PVA/PSBMA-PA- Li_2SO_4

hydrogel as electrolyte.

S3. Measurement of ionic conductivity

The conductivity of the hydrogel electrolytes was measured by the impedance spectrum over a frequency range from 0.1 Hz to 10^5 Hz. Typically, a piece of the hydrogel electrolyte was sandwiched between two stainless steel meshes. The area (S) of the electrolyte was 3 cm^2 and the distance (L) between the two stainless steel meshes was 0.2 cm. Bulk resistance R (Ω) was determined by the intercept with the real axis. Ionic conductivity σ (mS cm^{-1}) was calculated by the following formula:

$$\sigma = L / (R \times S) \quad (1)$$

S4. Characterizations

Fourier transform infrared (FT-IR) spectra was recorded on a Spectrum One spectrometer (PerkinElmer, U.S.A). The morphology of electrolytes was examined by using FE-SEM (Ultra Plus, Carl Zeiss) at an acceleration voltage of 5 kV. The crystal structure of the material was determined by X-ray diffraction (XRD, D/Max-2400, Science) equipped with Cu Ka radiation ($k=1.5418 \text{ \AA}$). The thermal stability of the samples was performed on a thermogravimetric analyser (PerkinElmer, USA).

S5. Electrochemical measurements

The electrochemical performances of the two-electrode supercapacitor devices were evaluated by using a CHI660D electrochemical workstation (Chenghua, Shanghai, China). Electrochemical impedance spectroscopy (EIS) measurements were conducted at open circuit potential in the frequency range of 100000 Hz to 0.1 Hz with an alternate voltage amplitude of 5 mV.

The specific capacitance of the electrode (C_s) was calculated according to follow formulas:

$$C_s = I \Delta t / m \Delta V \quad (2)$$

where I , Δt , m , ΔV and h are the discharge current, discharge time, the total mass of two pieces of active electrodes, the voltage changes upon discharging (excluding the IR drop) and h is the thickness of the device including the two working electrodes and the active material, respectively. Similarly, the energy density (E_A , Wh kg⁻¹) and power density (P_A , W kg⁻¹) were estimated using the follow formulas:

$$E_A = C_s \Delta V^2 / 8 \quad (3)$$

$$P_A = E_A / \Delta t \quad (4)$$

S6. Strain Sensing Performance Test

The real-time resistance signals and movements of the human body were recorded by connecting the ends of the hydrogel samples (size: 40 mm×10 mm×1.4 mm) with wires and adhering them directly to the joints of the human body, and then connecting the wires to the electrochemical workstation device. Resistance changes were recorded by measuring the I-t curve at a constant voltage of 1 V through the electrochemical workstation device. The relative resistance change and sensitivity at different strains were calculated by the following equation:

$$\Delta R/R_0 = (R - R_0) / R_0 \times 100\% \quad (5)$$

where R_0 is the original resistance at no strain and R is the real-time resistance at a certain deformation.

S7. Configuration of artificial seawater

The high salt water was composed of NaCl (26.7 g L⁻¹), KCl (7 g L⁻¹), MgSO₄ (3.2 g L⁻¹), MgCl₂ (2.3 g L⁻¹), CaCl₂ (1.15 g L⁻¹), and distilled water. The solution with different pHs was regulated by hydrochloric acid and sodium hydroxide. Distilled water (18.25 MΩ) was used in the experiment directly [S1].

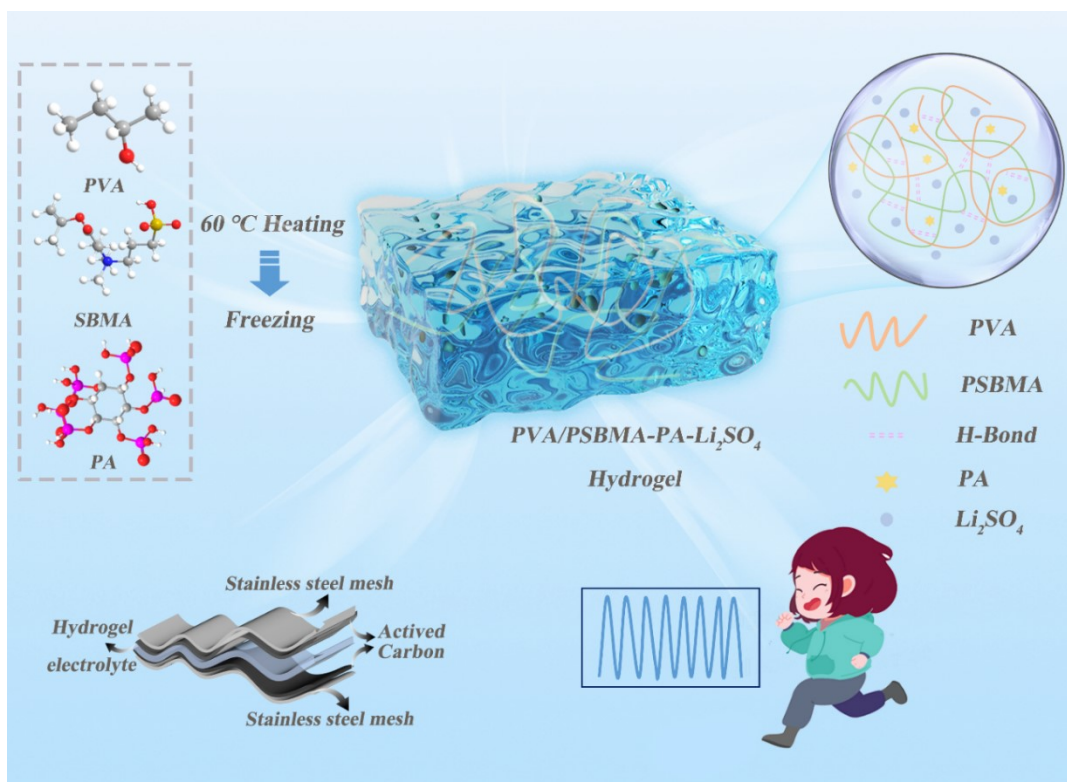


Fig. S1 Schematic diagram of the synthesis PVA/PSBMA-PA-Li₂SO₄ hydrogel electrolyte.

In the hydrogel, the PVA provides a solid backbone based on its inherent property of easy film formation, and the zwitterionic groups carried by PSBMA can act as an ionic conduction network and build a fast channel for ion transport. PA enhances the hydrogen bonding between the PVA chains while providing the acidic environment required for the protonation of -SO₃H in PSBMA. The Li₂SO₄ as an inorganic salt leading to an ionic cross-linked network due to the formation of intra- and inter-chain ionic contacts. Finally, freeze-thaw cycles were performed at -20 °C and room temperature to obtain physically cross-linked PVA/PSBMA-PA-Li₂SO₄ hydrogels with dual network structure.



Fig. S2 The diagram of hydrogel stretching.

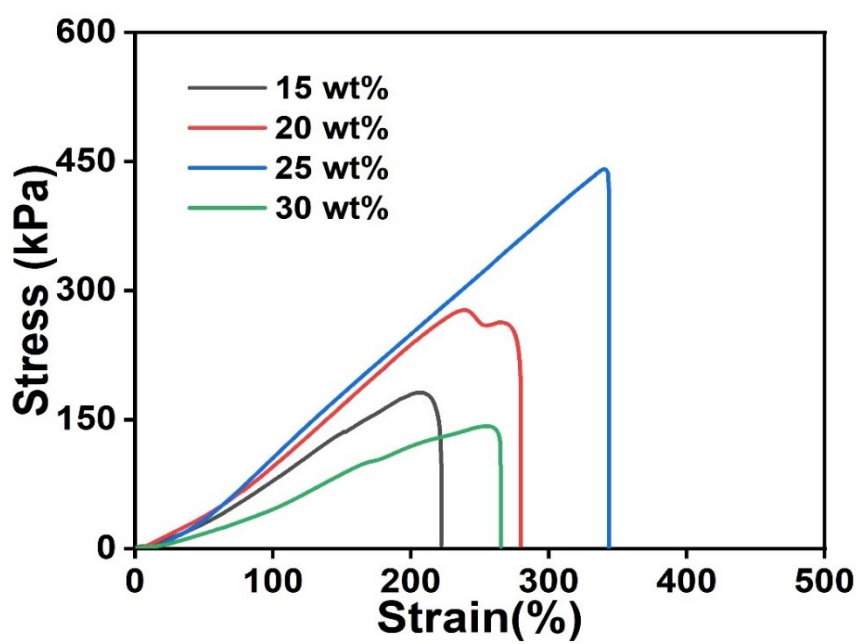


Fig. S3 Stress-strain curves of PVA/PSBMA-PA hydrogel with different contents of PA.

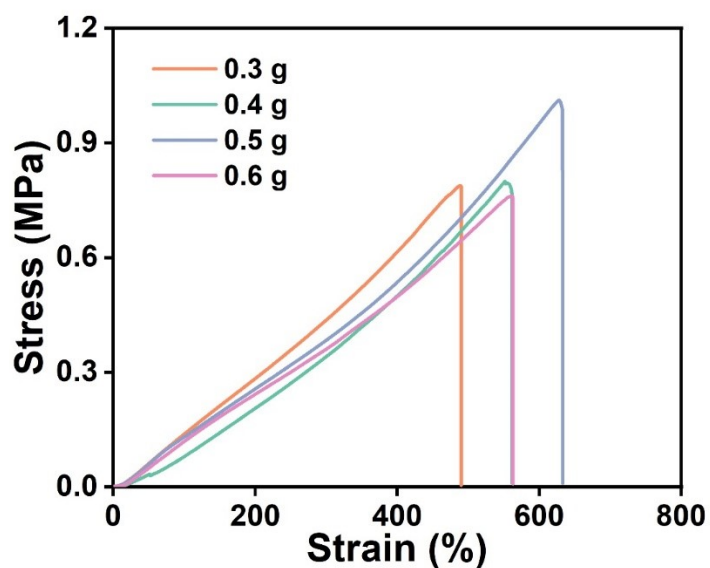


Fig. S4 Stress-strain curves of PVA/PSBMA-PA- Li_2SO_4 hydrogel with different contents of Li_2SO_4 .

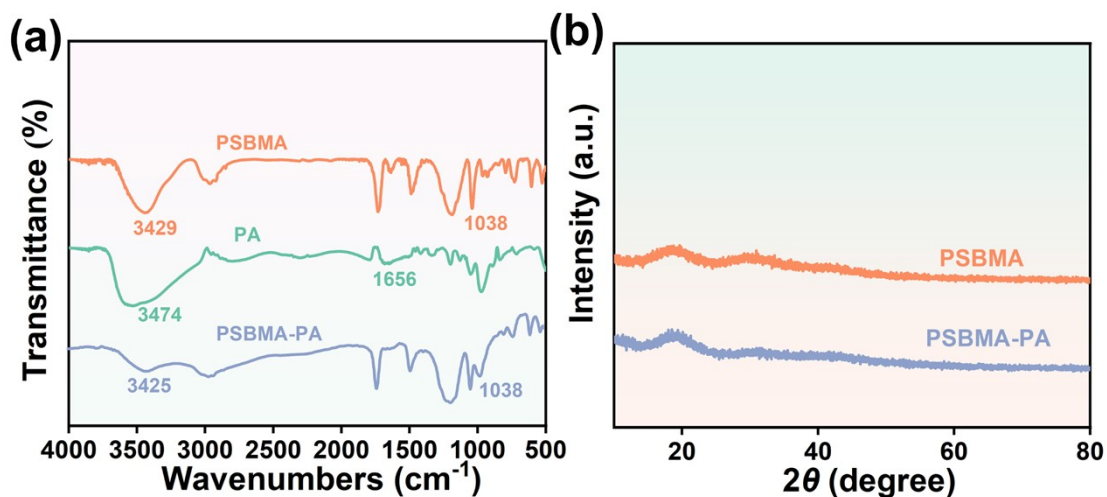


Fig. S5 (a) FTIR spectra of PSBMA, PA, and PSBMA-PA, (b) XRD spectra of PSBMA and PSBMA-PA.

As shown in Fig. S5a, the stretching vibration peak of O-H in hydroxyl groups shifted from 3429 cm^{-1} to 3425 cm^{-1} , indicating the formation of extensive hydrogen bonds. Meanwhile, the characteristic absorption peak of sulfonate groups at 1038 cm^{-1} weakened, further confirming the protonation of $-\text{SO}_3^-$ groups. As shown in Fig. S5b, with the introduction of PA, the crystalline domains in the PSBMA-PA hydrogel decreased, while the amorphous regions increased.

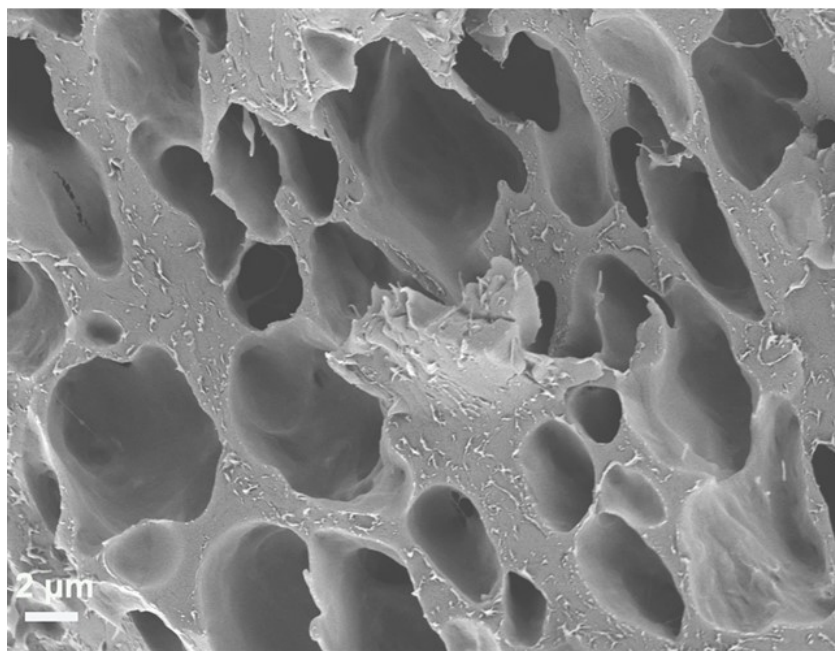


Fig. S6 The SEM images of PVA/PSBMA-PA hydrogel.

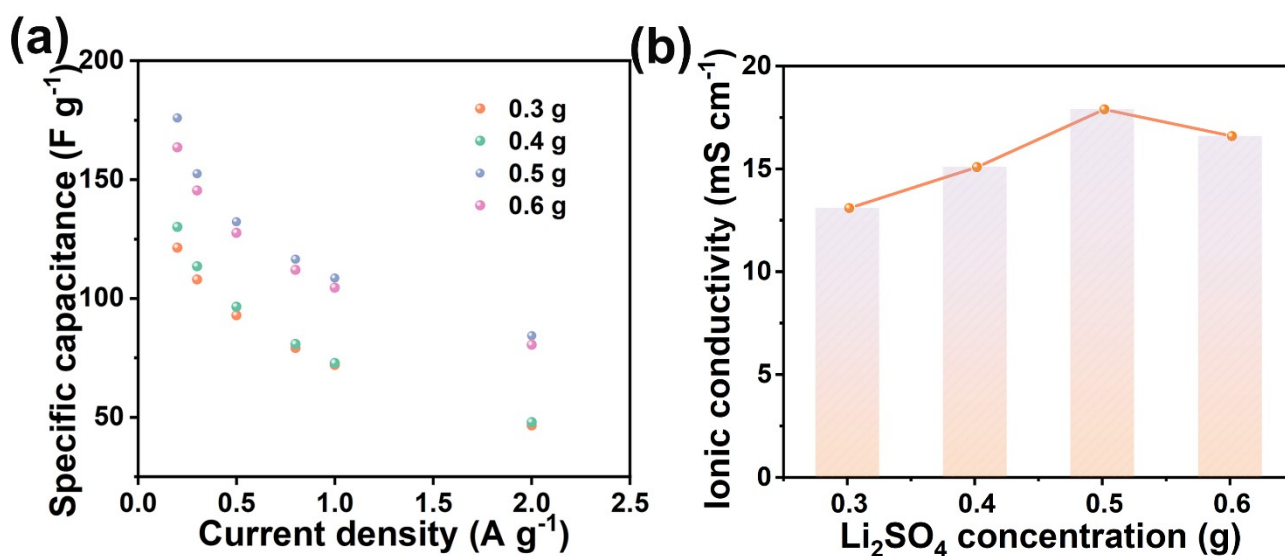


Fig. S7 (a) Rate capability of PVA/PSBMA-PA-Li₂SO₄ hydrogel-based FSCs, (b) Ionic conductivity of PVA/PSBMA-PA-Li₂SO₄ hydrogel.

The mass specific capacitance (**Fig. S7a**) of the PVA/PSBMA-PA-Li₂SO₄ hydrogel-based FSC calculated from the GCD curves shown that FSC with 0.5 g of Li₂SO₄ has a high specific capacitance of 175.9 F g⁻¹, which were better than those assembled from the FSCs prepared at 0.3 g, 0.4 g and 0.6 g of Li₂SO₄ content. The ionic conductivity of PVA/PSBMA-PA-Li₂SO₄ hydrogel calculated from their Nyquist curves shown that the hydrogel prepared at 0.5 g of Li₂SO₄ had a highest ionic

conductivity of 17.9 mS cm^{-1} (**Fig. S7b**). When the content of Li_2SO_4 is increased to 0.5 g, the number of free-moving ions in the hydrogel electrolyte increases and the electrochemical performance is improved, but when the content of Li_2SO_4 in the hydrogel is increased to 0.6 g, the addition of excess Li_2SO_4 leads to the deposition of lithium salts, which blocks the ion channels, causing the electrochemical performance of the hydrogel to decrease.

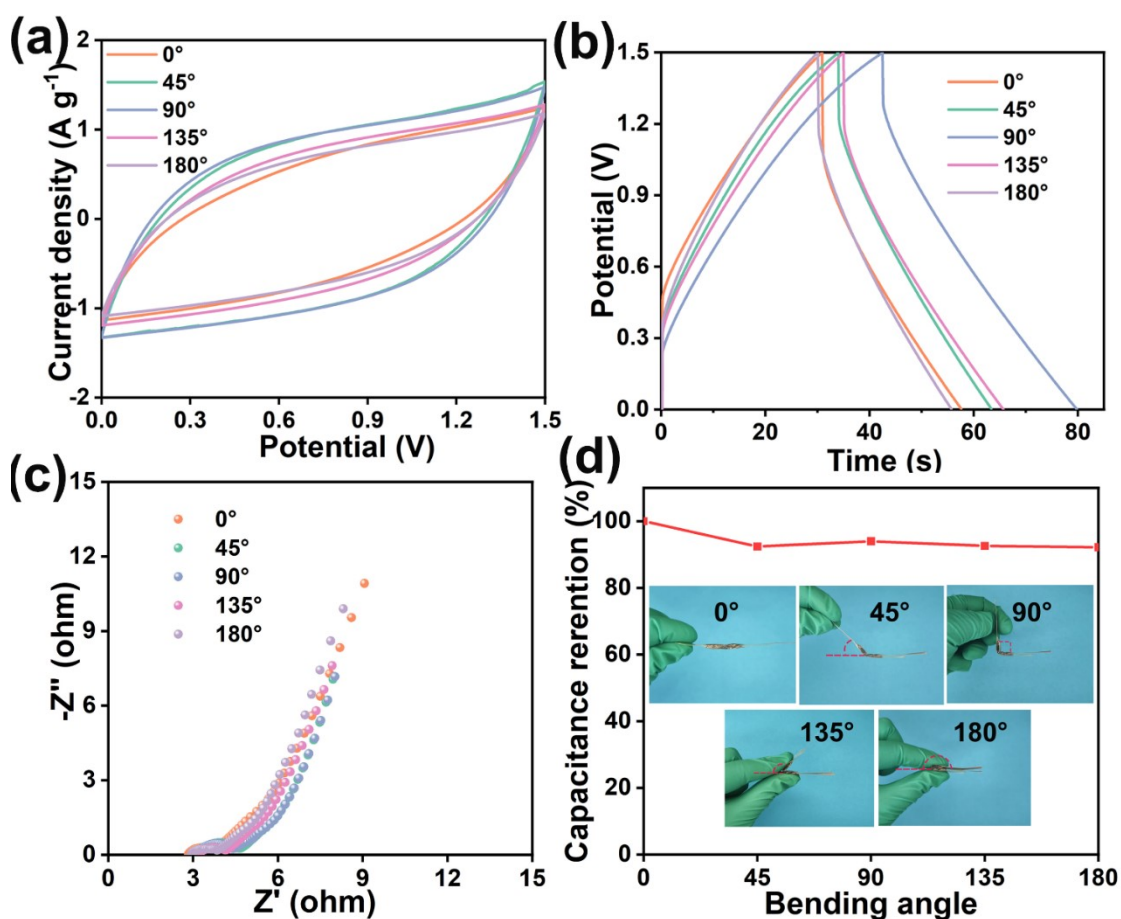


Fig. S8 Electrochemical performance of PVA/PSBMA-PA-Li₂SO₄ hydrogel based FSC at different bending angles (0°, 45°, 90°, 135°, 180°): (a) CV curves, (b) GCD curves, (c) Nyquist curves, (d) Capacitance retention.

The electrochemical properties of PVA/PSBMA-PA-Li₂SO₄ hydrogel-based FSCs were tested by measuring them at different bending angles to assess the practical application capability of the hydrogels. **Fig. S8a** shows the CV curves of the FSCs based on the PVA/PSBMA-PA-Li₂SO₄ hydrogel at 50 mV s⁻¹ for bending at 0°, 45°, 90°, 135° and 180°. All of the CV curves have similar shapes when bending at different bending angles. **In Fig. S8b**, the GCD curves of PVA/PSBMA-PA-Li₂SO₄ hydrogel-based FSCs bent at 0°, 45°, 90°, 135° and 180° at 0.8 A g⁻¹ are shown. The shapes of the GCD curves are also approximated at different bending angles, although their charge-discharge times are somewhat different. The Nyquist curves of PVA/PSBMA-PA-Li₂SO₄ hydrogel-based FSCs at 0°, 45°, 90°, 135°, and 180° are similar (**Fig. S8c**), which indicate that they have excellent ionic conductivity at different bending angles. This suggests that the capacitance of hydrogel electrolytes in

the bent state is similar to electrochemical processes. The capacitance retention was calculated based on the GCD curves, as shown in Fig. S8d.

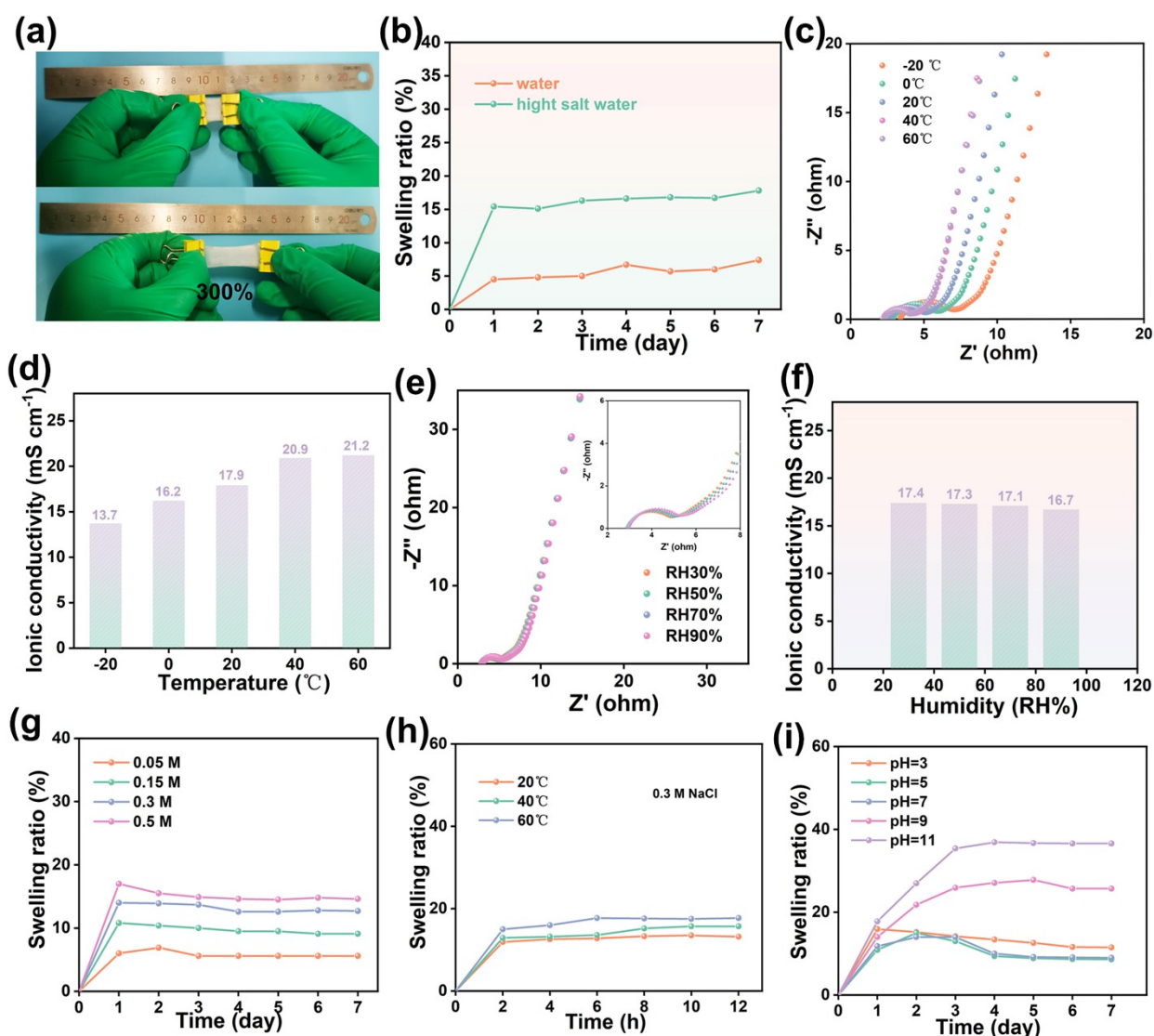


Fig. S9 (a) Tensile and (b) anti-swelling tests of hydrogel after 5,000-cycle stability testing; (c) EIS curves and (d) Ionic conductivities of PVA/PSBMA-PA- Li_2SO_4 hydrogel-based FSCs under different temperatures; (e) EIS curves and (f) Ionic conductivities of PVA/PSBMA-PA- Li_2SO_4 hydrogel-based FSCs under different humidities; Swelling properties of PVA/PSBMA-PA- Li_2SO_4 hydrogels under (g) different salt concentrations, (h) different temperatures, and (i) different pH conditions.

As shown in Fig. S9a and S9b, the hydrogel could still be stretched up to 300%, while exhibiting swelling ratios of 7.4% in deionized water and 17.8% in high-salt aqueous solution after 7 days. This

phenomenon may be attributed to the degradation of chemical crosslinks (e.g., covalent bonds) during repeated charge/discharge cycles, which loosens the polymer network and consequently exacerbates swelling.

EIS (Electrochemical Impedance Spectroscopy) tests on the PVA/PSBMA-PA-Li₂SO₄ hydrogel-based supercapacitor were conducted under different temperatures in Fig. S9c. The ionic conductivity at 60°C (21.2 mS cm⁻¹) is significantly higher than that at -20°C (13.7 mS cm⁻¹), indicating that elevated temperature accelerates ion migration in the hydrogel, thereby enhancing its capacitive performance and reducing resistance (Fig. S9d). EIS tests on the PVA/PSBMA-PA-Li₂SO₄ hydrogel-based supercapacitor were also tested under different humidities (Fig. S9e). The ionic conductivity at RH30% (17.4 mS cm⁻¹) is higher than that at RH90% (16.7 mS cm⁻¹), indicating that excessive humidity will dilute the gel ion concentration, resulting in a decrease in ionic conductivity (Fig. S9f).

The swelling performance of PVA/PSBMA-PA-Li₂SO₄ hydrogels were tested at different salt concentrations (Fig. S9g), temperatures (Fig. S9h), and pH conditions (Fig. S9i). As shown in Fig. S9g, the swelling performance of PVA/PSBMA-PA-Li₂SO₄ hydrogel soaked in different concentrations of NaCl solution for seven days is compared, and it can be seen that with the higher concentration of NaCl solution, the larger the swelling ratio of PVA/PSBMA-PA-Li₂SO₄ hydrogel, which is due to the fact that in the electrolyte solution, the surface charge of the hydrogel is shielded by the electrolyte salt of small molecules, which enhances the hydration of zwitterion, thereby promoting osmosis and swelling. As shown in Fig. S9h, the PVA/PSBMA-PA-Li₂SO₄ hydrogel was immersed in 0.3 M NaCl solution, and swelling performance tests were conducted at 20°C, 40°C, and 60°C, respectively. The results show that temperature promotes the swelling of the hydrogel, which may be attributed to the fact that increased temperature enhances the thermal motion ability of the polymer chains, making the crosslinked network more expandable and allowing solvent molecules to penetrate more easily. Consequently, this accelerates the swelling rate and improves the equilibrium swelling ratio. [Mater. Sci. Eng., C 2021, 127, 112208]. As shown in Fig. S9i, the PVA/PSBMA-PA-

Li_2SO_4 hydrogel was immersed in solutions with different pH values for 7 days. The equilibrium swelling ratio of the hydrogel gradually increased with rising pH. This is because, in an acidic environment, the $-\text{SO}_3^-$ groups become protonated, causing the hydrogel to exhibit polycationic behavior. In contrast, under alkaline conditions, alkaline ions induce an anti-polyelectrolyte effect and promote dissociation within and between PSBMA chains, leading to an enhanced swelling ratio of the hydrogel. [Adv. Funct. Mater. 2021, 32, 2107404].

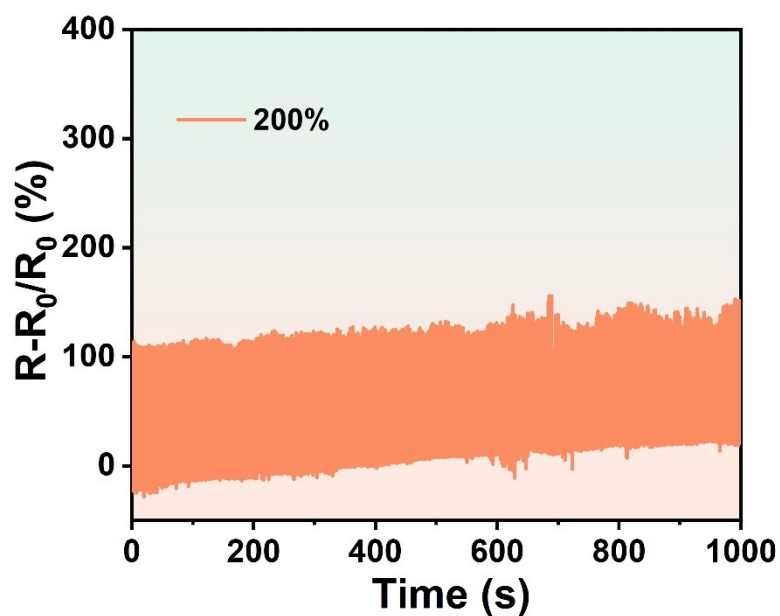


Fig. S10 Durability test under 1000 cycles of stretching at 200% strain

The hydrogel sensor underwent stretch-release cycles at 200% strain, demonstrating relatively stable resistance changes over 1000 cycles (Fig. S10). The slight increase in resistance may be attributed to unstable stress or hysteretic strain generated during prolonged repeated stretching that did not fully recover immediately, thereby leading to elevated resistance. Overall, the strain sensor demonstrated excellent signal stability and reproducibility throughout the cycling tests, with a corresponding gauge factor (GF) of 0.65.

Table S1. Comparison of electrochemical properties of our device with recently reported gel-based supercapacitors.

Materials	Specific Volume	Cyclic Stability	Specific Capacitance (W kg ⁻¹)	Energy Density (Wh kg ⁻¹)	Refs.
PVA/PSBMA-PA-Li ₂ SO ₄	175.9 F g ⁻¹ (0.2 A g ⁻¹)	78% (5000 cycles)	150	13.7	This work
PVA / PIL gel electrolyte	34.2 F g ⁻¹ (50 mA g ⁻¹)	79% (5000 cycles)	560	12.8	[S2]
B-PVA/KCl/GO gel	156 F g ⁻¹ (0.3 A g ⁻¹)	—	492.7	5	[S3]
Reinforced LiClO ₄ Gel	29.5 F g ⁻¹ (1 A g ⁻¹)	—	95.97	7.87	[S4]
Neutral pH Na ₂ SO ₄ /glycerol/PVA polymer hydrogel electrolyte	54.7 F g ⁻¹ (0.5 A g ⁻¹)	—	—	7.6	[S5]
HA-GPE	130.3 F g ⁻¹ (0.5 A g ⁻¹)	90.1% (5000 cycles)	67.84	8.99	[S6]
PVA/NaCl/glycerol Gel	52.9 F g ⁻¹ (0.5 A g ⁻¹)	—	250	7.4	[S7]
Li-AG/PAM gel electrolyte	84.7 F g ⁻¹ (0.2 A g ⁻¹)	—	50	1.75	[S8]
Poly(arylene ether sulfone)/poly(vinylpyrrolidone) composite membranes	136.05 F g ⁻¹ (0.5 A g ⁻¹)	97% (5000 cycles)	115.77	4.47	[S9]

Table S2. Comparison of electrochemical properties of our device with recently reported gel-based supercapacitors.

Materials	tensile strength	conductivity	swelling ratio (in water)	Refs.
PVA/PSBMA-PA-Li ₂ SO ₄	631%	17.9 mS cm ⁻¹	4%	This work
SBMA/PVA/TA (SPT) hydrogel	287.52%	0.06 S m ⁻¹	≈-15%	[S10]
P(SBMA- <i>co</i> -HEMA) hydrogel	287%	3.0 S/m	150%	[S11]
PVA/Gel/TA/MXene hydrogel	400%	1.4 S/m	16.6 %	[S12]
P(AA-MEA)-CS-Fe	462%	0.326 S/m	13%	[S13]
Starch/PVA/AlCl ₃ /[Emim]Ac (SPAЕ) hydrogels	530%	2.75 S/m	25%	[S14]

References

- [S1] J. Ren, Y. Liu, Z. Wang, S. Chen, Y. Ma, H. Wei and S. Lü, An Anti-Swellable Hydrogel Strain Sensor for Underwater Motion Detection, *Adv. Funct. Mater.* 32 (2021) 2107404.
- [S2] C. Ramasamy, P. Porion, L. Timperman and M. Anouti, An amide based polyvinyl alcohol / protic ionic liquid (PVA / PIL) gel electrolyte for supercapacitor applications, *Synth. Met.*, 2023, 299, 117469.
- [S3] H. Peng, Y. Lv, G. Wei, J. Zhou, X. Gao, K. Sun, G. Ma, Z. Lei, A flexible and self-healing hydrogel electrolyte for smart supercapacitor, *J. Power Sources*, 2019, 431, 210-219.
- [S4] R. Na, G. Huo, S. Zhang, P. Huo, Y. Du, J. Luan, K. Zhu and G. Wang, A novel poly(ethylene glycol)-grafted poly(arylene ether ketone) blend micro-porous polymer electrolyte for solid-state electric double layer capacitors formed by incorporating a chitosan-based LiClO_4 gel electrolyte, *J Mater Chem A*, 2016, 4, 18116-18127.
- [S5] A. G. Sánchez-Valdez, S. M. Parra-Arciniega, E. M. Sánchez-Cervantes and L. C. Torres-González, Neutral pH Na_2SO_4 /glycerol/PVA polymer hydrogel electrolyte prepared at room temperature for activated carbon supercapacitors, *J. Solid State Electrochem.*, 2023, 27, 2917–2925.
- [S6] R. Na, Y. Liu, N. Lu, S. Zhang, F. Liu and G. Wang, Mechanically robust hydrophobic association hydrogel electrolyte with efficient ionic transport for flexible supercapacitors, *Chem. Eng. J.*, 2019, 374, 738-747.
- [S7] S. Peng, X. Jiang, X. Xiang, K. Chen, G. Chen, X. Jiang and L. Hou, High-performance and flexible solid-state supercapacitors based on high toughness and thermoplastic poly(vinyl alcohol)/NaCl/glycerol supramolecular gel polymer electrolyte, *Electrochim. Acta*, 2019, 324, 134874.
- [S8] T. Lin, M. Shi, F. Huang, J. Peng, Q. Bai, J. Li and M. Zhai, One-pot synthesis of a double-network hydrogel electrolyte with extraordinarily excellent mechanical properties for a highly compressible and bendable flexible supercapacitor, *ACS Appl. Mater.*, 2018, 10, 29684–29693.

- [S9] P. Huo, Y. Liu, R. Na, X. Zhang, S. Zhang and G. Wang, Quaternary ammonium functionalized poly(arylene ether sulfone)/poly(vinylpyrrolidone) composite membranes for electrical double-layer capacitors with activated carbon electrodes, *J. Membr. Sci.*, 2016, 505, 148-156.
- [S10] L. Wu, S. Wang, J. Mao, Z. Guo and Y. Hu, Dual network zwitterionic hydrogels with excellent mechanical properties, anti-swelling, and shape memory behaviors, *Eur. Polym. J.*, 2023, 197, 112373.
- [S11] Y. Shi, Y. Ding, W. Wang and D. Yu, High performance zwitterionic hydrogels for ECG/EMG signals monitoring, *Colloids Surf. A Physicochem. Eng. Asp.*, 2023, 675, 132081.
- [S12] Y. Chen, W. Guo, N. Chen, Y. Liu, X. Wan, T. Wang, Z. Zhou, Y. Jin and G. Li, Skin-inspired MXene-based polyvinyl alcohol/gelatin organic hydrogel with good anti-drying, anti-swelling properties and high sensitivity, *Sens. Actuators A Phys.*, 2025, 383, 116231,
- [S13] Z. Zhao, X. Qin, L. Cao, J. Li and Y. Wei, Chitosan-enhanced nonswelling hydrogel with stable mechanical properties for long-lasting underwater sensing, *Int. J. Biol. Macromol.*, 2022, 212, 123-133.
- [S14] L. Lu, Z. Huang, X. Li, X. Li, B. Cui, C. Yuan, L. Guo, P. Liu and Q. Dai, A high-conductive, anti-freezing, antibacterial and anti-swelling starch-based physical hydrogel for multifunctional flexible wearable sensors, *Int. J. Biol. Macromol.*, 2022, 213, 791-803.